Title

A strategy to increase phosphor brightness: Application with Ce^{3+}–doped $Gd_3Sc_2Al_3O_{12}$

Journal

Journal of Luminescence, 190

ISSN

00222313

Authors

Devys, Lucie
Dantelle, GÃ©raldine
Laurita, Geneva
et al.

Publication Date

2017-10-01

DOI

10.1016/j.jlumin.2017.05.035

Peer reviewed

A Strategy to Increase Phosphor Brightness: Application with Ce^{3+}-doped $Gd_3Sc_2Al_3O_{12}$

Lucie Devys*, Géraldine Dantelle[‡,]*, Geneva Laurita[&], Estelle Homeyer[#], Isabelle Gautier-Luneau[‡], Christophe Dujardin[#], Ram Seshadri[&], Thierry Gacoin*

*Laboratoire de Physique de la Matière Condensée, Ecole Polytechnique
Route de Saclay – 91128 Palaiseau, France

[‡] Institut Néel CNRS, UPR 2940/Université Grenoble Alpes
25 Av. des Martyrs – 38 042 Grenoble Cedex 09, France

[&]Materials Research Laboratory, University of California Santa Barbara
CA 93106-5121, USA

[#]Institut Lumière Matière, UMR5306 Université Lyon 1-CNRS, Université de Lyon,
69622 Villeurbanne Cedex, France

Corresponding author: geraldine.dantelle@neel.cnrs.fr

Key words: phosphors, lighting, cerium, brightness, luminescence

Abstract

$Y_3Al_5O_{12}$ (YAG) doped with Ce^{3+} ions is widely used as a phosphor for the generation of white light in LEDs. However, the material presents intrinsic drawbacks: (1) a yellow emission band lacking a red component, leading to a "cold" white light and (2) limited cerium incorporation (~ 3 mol.%), resulting in poor absorption and thus limiting the external quantum efficiency (EQE) of the LED device. In order to increase phosphor absorption and thus phosphor brightness, we propose here an original strategy based on the increase of Ce content in a phosphor compound, while preserving a high internal luminescence quantum yield. For this purpose, we introduce Ce^{3+}-doped $Gd_3Sc_2Al_3O_{12}$ (GSAG:Ce). $Gd_{3(1-x)}Ce_{3x}Sc_2Al_3O_{12}$ polycrystalline samples were prepared through a solid-state microwave-assisted reaction, with x varying from 0 to 0.5; Ce^{3+} ions can be incorporated into the GSAG matrix with a concentration up to approximately x = 0.18 (i.e. 18 mol.%) without the formation of a parasitic phase. The maximum emission wavelength is located at 573 nm for a doping concentration of x = 0.1, giving an orange feature to the emission. The internal luminescence quantum yield (Φ) is 52 % for Ce concentration up to x = 0.03. The EQE, which is proportional to the product of Φ by the Ce concentration when considering a thin transparent phosphor layer is predicted to be about 30 % stronger when using GSAG doped with 10 mol.% Ce (x=0.1), with respect to YAG doped with 2 mol.% Ce (x=0.02).

1. Introduction

Yttrium aluminium garnet (YAG) doped with Ce^{3+} is known as an efficient yellow phosphor with high internal luminescence quantum yield (>90%) and perfect photostability.[1] One of its broad absorption bands peaks at 450 nm and matches perfectly the blue-emitting LEDs for the generation of white light. However, the emission wavelength lacks a red component, producing a so-called "cold" white light. Moreover, the quantity of Ce^{3+} ions that can be incorporated into the YAG matrix is small due to the mismatch between the Ce^{3+} ionic radius (1.143 Å for a coordination number of 8) and the substituted Y^{3+} ionic radius (1.019 Å for a coordination number of 8): the maximum concentration is reported as 3 at.% when YAG:Ce is synthesized by solid state reaction.[2] This results in a small absorption of the blue light of the GaN diode, and a large amount of powder or ceramics is required to acquire the appropriate yellow component from the device. Additional drawbacks include re-absorption and strong scattering that reduces the external quantum efficiency (EQE) of these white LED devices.

Several strategies have been employed to increase the phosphor absorption. T. Hussain *et al.* report the grafting of Au nanoparticles onto YAG nanoparticles in order to enhance absorption via plasmonic effects.[3] Their results indicate a large enhancement of the PL intensity of YAG:Ce after Au nanoparticle modification. Other groups propose to control the size of YAG grains to limit light back-scattering.[4] Another method consists of controlling light propagation within the phosphor film to generate light in the desired direction.[5,6]

Herein we investigate a different strategy which consists in increasing the phosphor brightness by increasing the Ce doping concentration while ensuring that the internal luminescence quantum yield remains high. For this purpose, we use the $Gd_3Sc_2Al_3O_{12}$ matrix, also called GSAG, as an alternative to YAG for the incorporation of the doping ions. GSAG has a larger unit cell parameter than that of YAG (a = 12.39 Å [7] versus 12.01 Å [2], respectively) that favours the insertion of Ce^{3+} ions. One would thus expect a higher solubility of Ce^{3+} ions into the structure and thus a stronger absorption that could lead to a higher EQE. In addition, GSAG crystallizes in the garnet structure, which should allow preserving the spectroscopic properties of Ce^{3+} in terms of excitation and emission wavelengths. Relatively few papers report the formation of the GSAG phase. Most report on GSAG doped with Cr^{3+} for laser applications,[8,9,10] while others utilize GSAG doped with Ce^{3+} for scintillation applications for conversion of the γ-rays and neutrons into light.[11,12,13] Here we present the synthesis of GSAG:Ce crystalline powders as well as their structural and optical characteristics. As the goal is to find an alternative to YAG:Ce for lighting applications, the results obtained on GSAG:Ce will be discussed with respect to those obtained with YAG:Ce.

2. Experimental methods

2.1. Microwave-assisted GSAG:Ce preparation[14]

Samples were prepared by mixing Gd_2O_3 (Alfar Aesa, 99.99%), CeO_2 (Cerac, 99.9%), Sc_2O_3 (Stanford Materials Corporation, 99.99%), Al_2O_3 (Sumitomo AKP-50, >99.99%) in stoichiometric proportions for $Gd_{3(1-x)}Ce_{3x}Sc_2Al_3O_{12}$ with x=0 , 0.005 , 0.01 , 0.02 , 0.03 , 0.04 , 0.05 , 0.06 , 0.1, 0.2, and 0.5 for a total mass of 1 g. These samples will be referred to as GSAG:xCe in the following. The powders were ground in an alumina mortar with 5 wt.% BaF_2 (Cerac, 99%) and 0.5 wt.% NH_4F (Sigma-Aldrich, 99.9%) as flux. The mixture was decanted into a small alumina crucible and inserted into a larger alumina crucible filled with 6.5 g of granular carbon (Darco 12 to 20 mesh, Sigma-Aldrich) used as the microwave susceptor. Both crucibles were capped with an alumina lid. The system was placed in a high temperature alumina isolator and heated in a domestic microwave oven for 18 min at a power level between 750 and 850 W.

2.2 YAG:Ce preparation

The properties of the Ce-doped GSAG are compared to those of the Ce-doped YAG synthesized by solid state according to the procedure reported in [2]. Briefly, Y_2O_3, Al_2O_3 and CeO_2 were ground together with 5% by mass BaF_2 and 0.5% by mass NH_4F acting as sintering agents. The mixture was then placed in alumina crucibles and fired at 1500 °C for 5 h in an alumina tube furnace under 0.2 L/min 5% H_2/N_2 gas flow. $Y_{3(1-x)}Ce_{3x}Al_5O_{12}$ with x=0.01, 0.02 and 0.03 were prepared. These samples are referred to as YAG:xCe in the following. It is reported that conventional solid state and microwave assisted methods lead to YAG:Ce compounds with identical structural and optical properties,[14] allowing for the direct comparison of solid state YAG to microwave-assisted GSAG.

2.3 X-Ray diffraction

X-ray diffraction was performed on the GSAG:xCe samples using two different instruments. Samples where x = 0, 0.005, 0.01 – 0.06, 0.1, 0.2, and 0.5 were analysed using a Philips XPert diffractometer (λ_{Cu}=1.54056 Å). Samples where x = 0.005, 0.03, 0.06, and 0.1 were characterized using the 11-BM beamline at the Advanced Photon Source (APS) at Argonne National Laboratory (λ = 0.412154 Å). Lattice parameters and phase purity was determined through the LeBail method using the GSAS software package with EXPGUI.[15,16,17] Crystal structures were visualized using the VESTA suite of programs.[18] The interatomic distances in YAG and GSAG were calculated using Gretep software.[19]

2.4 Optical characterization

Luminescence properties were characterized on a Perkin-Elmer LS55 spectrophotometer on pellets. The pellets were prepared by grinding and pressing 200 mg of KBr (≥99%, FT-IR grade, Sigma-Aldrich) with 20 mg of every sample. The excitation was measured with an emission wavelength (λ_{em}) of 564 nm and by scanning from 300 nm to 540 nm. The emission was collected from 480 nm to 800 nm with an excitation wavelength (λ_{ex}) of 450 nm.

To measure the internal luminescence quantum yield, each sample was mixed with silicone GE RTV615A+B in a 0.2:1 ratio. A drop of the mixture was then deposited on a 1x1 cm quartz slide and heated at 150°C for 15 min to cure the silicone. The samples were inserted into an integrating sphere and excited at 457 nm with an Ar laser.

To measure the excited state lifetime as a function of temperature, the powder samples were placed into a cryostat, where the temperature can be varied from 77 to 873 K, and excited by a 444-nm pulsed laser. The emission, selected in a 500-600 nm range by two high- and low-pass filters, was collected into a PhotoMultiplier and amplified. The signal was then histogrammed using a multichannel counter with a resolution of 800 ps. For details of this experimental set-up and interpretation of the data see [20].

3. Results

3.1 Increased Ce solubility limit in GSAG

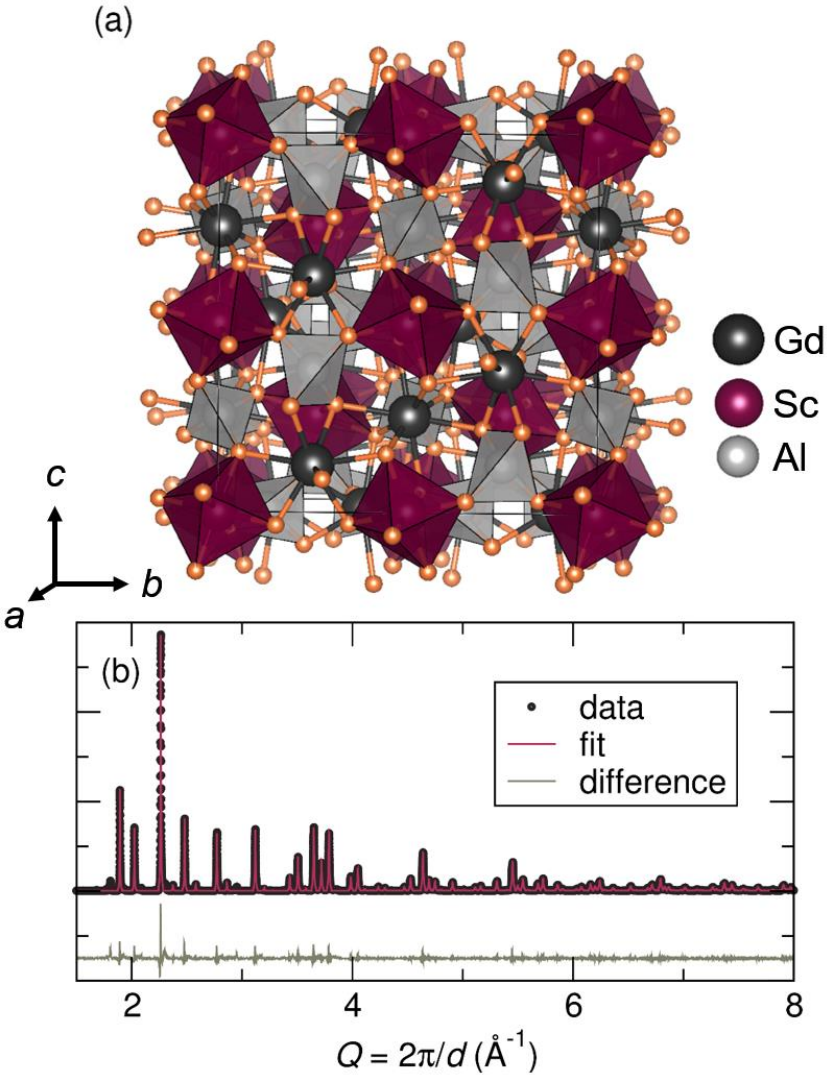

***Figure 1**: (a) Crystal structure of $Gd_3Sc_2Al_3O_{12}$ in the $Ia\bar{3}d$ space group with ScO_6 octahedra shown in maroon, AlO_4 tetrahedra in grey, O^{2-} in orange and Gd^{3+} in charcoal. (b) LeBail fit of the 11-BM data for $Gd_{2.7}Ce_{0.3}Sc_2Al_3O_{12}$ indicates the sample is phase pure and properly indexed by this space group.*

The GSAG compound, isostructural with YAG, crystallizes with the cubic garnet structure in $Ia\bar{3}d$ space group. The structure is constituted of AlO_4 tetrahedra, ScO_6 octahedra and Gd^{3+} in an 8-coordinated site, represented in **Figure 1a**. In order to determine the purity and lattice parameters of the synthesized GSAG:*x*Ce samples, powder X-ray diffraction data were recorded utilizing both a laboratory and synchrotron X-ray source. **Figure 1b** shows the LeBail fit to the diffraction pattern of $Gd_{2.7}Ce_{0.3}Sc_2Al_3O_{12}$ collected on 11BM, and is representative of the synchrotron data. No impurity phase was detected for this doping concentration (x = 0.1).

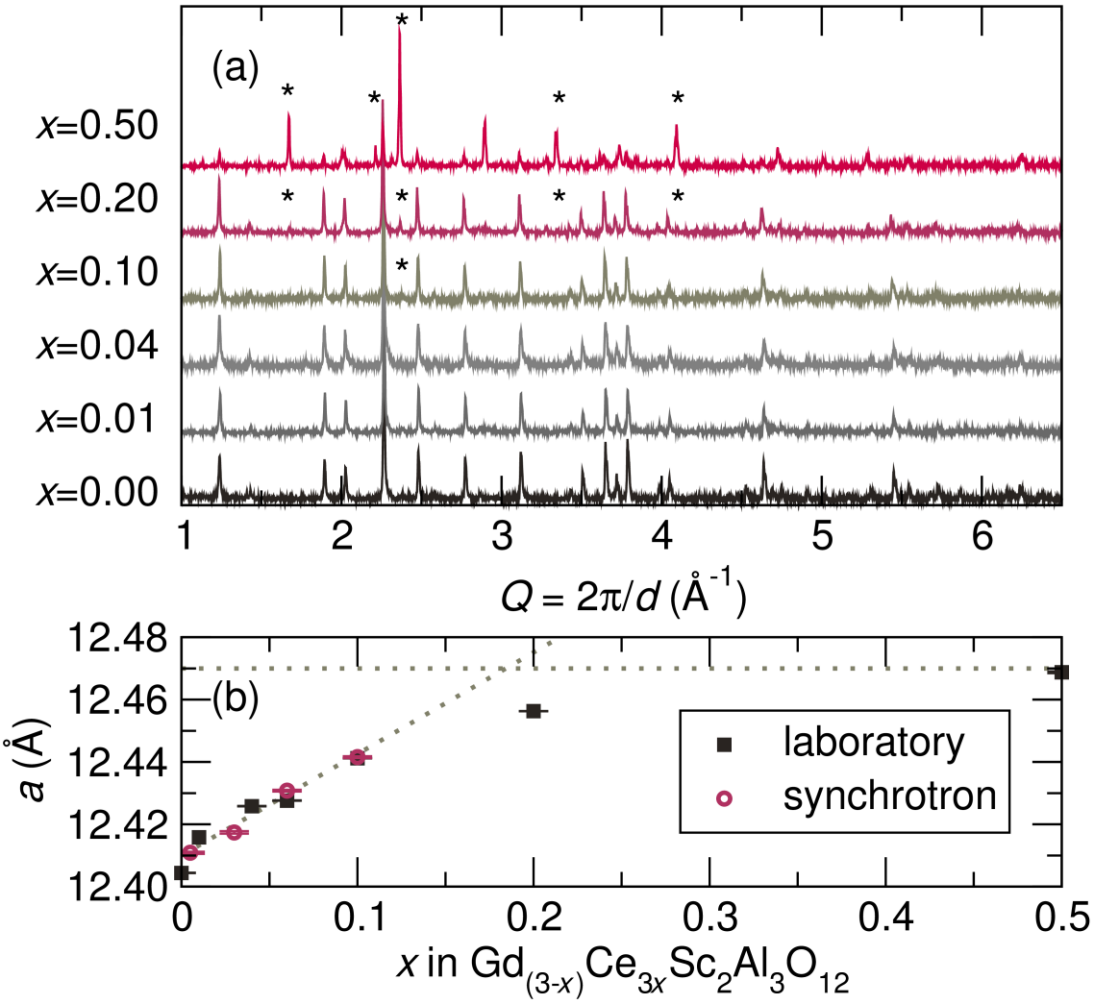

Figure 2: *(a) Laboratory powder X-Ray diffraction patterns of $Gd_{3(1-x)}Ce_{3x}Sc_2Al_3O_{12}$ for x varying from 0 to 0.5. The peaks indicated with * correspond to the $CeAlO_3$ perovskite phase. (b) Evolution of the unit cell parameter a of the GSAG:xCe phase as a function of the Ce concentration x, determined from X-ray laboratory source (black square) or synchrotron (maroon open circle).*

Laboratory X-ray diffraction data collected on Ce doping concentration x = 0, 0.005, 0.01 – 0.06, 0.1, 0.2, and 0.5 are shown in **Figure 2a**. In order to determine the maximum Ce concentration in GSAG, the evolution of the unit cell parameter a was studied as a function of the cerium concentration (**Figure 2b**). From x=0 to x=0.1, a varies linearly with x, as predicted by Vegard's law. For x=0.2 and 0.5, the value of a slightly increases, but deviates from Vegard-like behavior. This is correlated with the appearance of a secondary $CeAlO_3$ perovskite phase, indicated by * in **Figure 2a**. At these doping levels, Ce^{3+} does not enter the GSAG matrix and favors the formation of the perovskite phase. From this study, the limit of Ce solubility in the GSAG matrix is estimated to be close to 18 mol. %. This value is about 6 times higher than in the YAG matrix synthesized by solid state chemistry. For x varying from 0 to 0.1, only the GSAG phase is detected. For x=0.2, a small amount of the perovskite phase $CeAlO_3$ is visible, and for x=0.5, $CeAlO_3$ is the main phase observed.

3.2 Spectroscopic properties of Ce^{3+} in GSAG

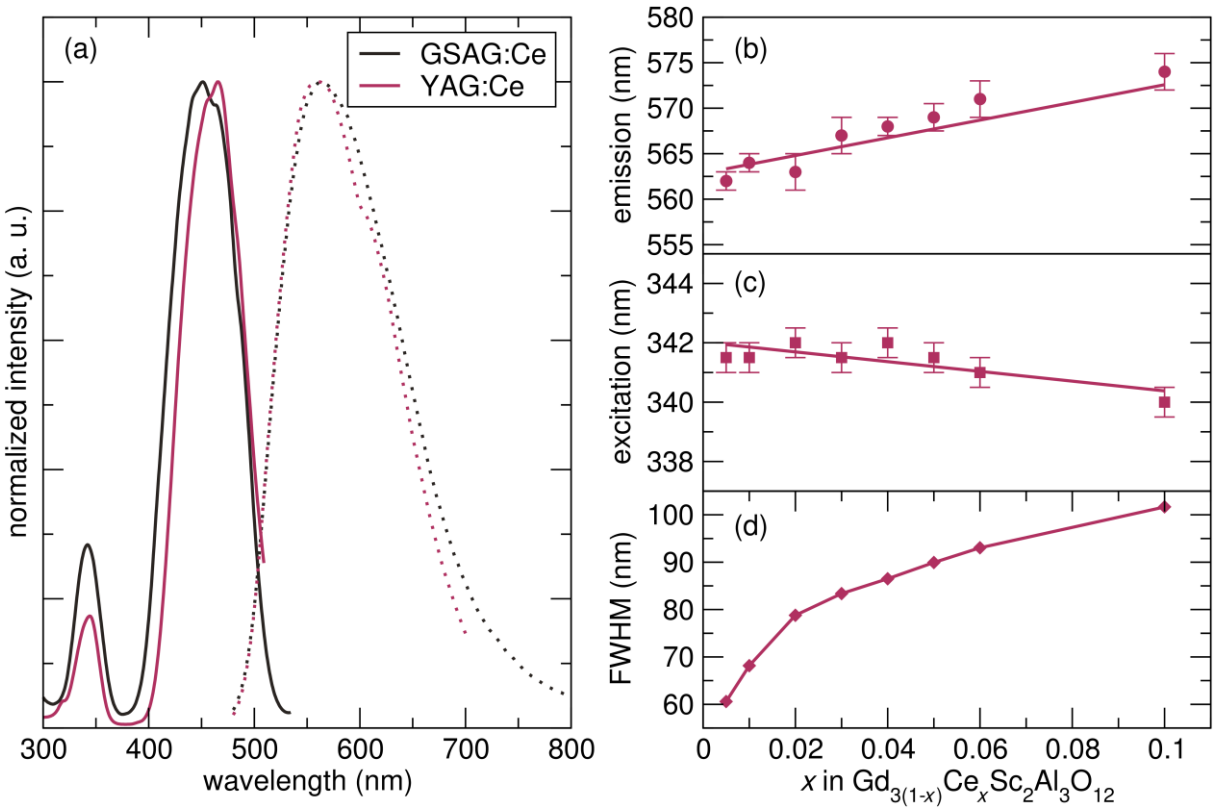

Figure 3: *(a) Excitation and emission spectra of GSAG:0.02Ce (black line) and YAG:0.02Ce (maroon line). The excitation spectra were recorded with an λ_{em} of 564 nm (GSAG:Ce) and 546 nm (YAG:Ce). The emission spectra were recorded with λ_{ex} of 450 nm (GSAG:Ce) and 457 nm (YAG:Ce). Evolution of the (b) emission and (c) excitation peak position and of the (d) excitation peak FWHM as a function of the doping concentration x in $Gd_{3(1-x)}Ce_{3x}Sc_2Al_3O_{12}$.*

The excitation and emission spectra of GSAG:0.02Ce and YAG: 0.02Ce samples are presented in **Figure 3a**, with λ_{em} = 564 nm and 546 nm, λ_{ex} = 450 nm and 457 nm, respectively. The peak shape of both spectra is the signature of Ce^{3+} ions. The two excitation peaks, at approximately 340 nm and 450 nm, correspond to the 4f→5d ($^2B_{1g}$) and 4f→5d($^2A_{1g}$) transitions, and the broad emission peak in the yellow range is associated to the 5d ($^2A_{1g}$) →4f transition. However, for the same Ce concentration of x = 0.02, the maximum of the main excitation peak of the GSAG is blue shifted (451 nm) compared to YAG (466 nm), while the maximum of the emission peak is slightly shifted to the red range (563 nm in GSAG compared to 561 nm in YAG).

The evolution of the maximum of the excitation and emission peak in Ce-doped GSAG, as well as the excitation peak FWHM, can be followed throughout the entire doping range of x (**Figure 3b-c**). The maximum of the emission peak significantly shifts towards the higher emission wavelength ($\Delta\lambda$ ~ 10 nm) as x increases, while the excitation peak remains at approximately the same position. However, the FWHM increases significantly with increasing Ce content. Note that this line broadening is asymmetrical, with a main broadening at longer wavelength. The observed optical properties arise from inter-configurational 4f→5d transitions of Ce^{3+}, which are sensitive to the crystal field splitting of the Ce^{3+} ion. Changes in the coordination environment of Ce induce changes in the crystal field, and thus a variation of the position of the excitation and emission bands. It has previously been reported that an increase of the radius of the ion in the dodecahedral site induces a lattice distortion, leading

to an increased splitting of the 5d levels and resulting in a red shift of the emission.[21,22] This is consistent with the red shift observed from YAG to GSAG as the ionic radius of Y^{3+} (1.019 Å for CN=8) is smaller than the one of Gd^{3+} (1.053 Å in CN=8), as well as the evolution of the emission band position with the increase of the Ce content as the ionic radius of Gd^{3+} is smaller than that of Ce^{3+} (1.143 Å in CN=8). The broadening of the excitation band prevents the observation of the red shift as expected.[22] This broadening with Ce concentration could result from inhomogeneous broadening of the crystal field due to distortions and also from possible effects of non-linear absorption dependence.

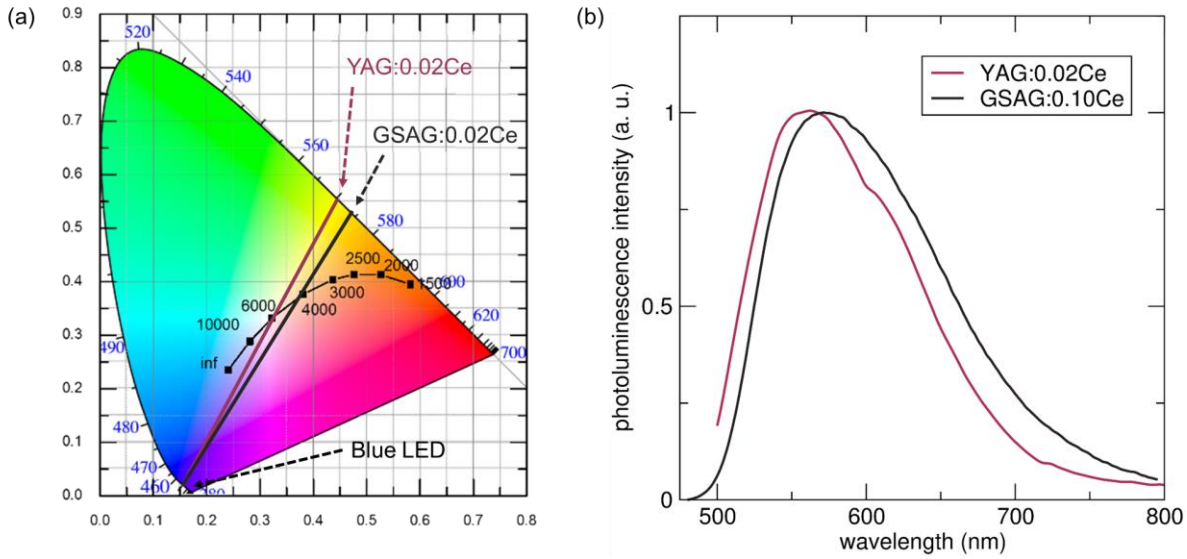

***Figure 4**: (a) CIE chromaticity diagram of potential devices utilizing YAG:0.02Ce and GSAG:0.1Ce. The lines correspond to simulated colors produced by mixing the emission of a blue LED with different quantities of YAG:0.02Ce powder (maroon line) or GSAG:0.1Ce powder (black line). The black curve corresponds to the black body radiation. (b) Emission spectra of YAG:0.02Ce and GSAG:0.1Ce for further comparison.*

The red shift associated with Ce doping of the GSAG matrix is highly beneficial for the generation of warmer white light. The combination of a blue GaN diode with YAG:Ce phosphors leads to a cold white light, encouraging people to search for red emitting phosphors.[23,24,25] However, a redshift in the emission maximum was observed with both the replacement of Y^{3+} with Gd^{3+} and the substitution of Ce^{3+}. The light color resulting from mixing blue and yellow emission generated either by YAG:0.02Ce or by GSAG:0.1Ce was estimated for different amounts of phosphor powder and plotted as Commission International de l'Éclairage (CIE) coordinates (**Figure 4a**) to evaluate the potential of GSAG:Ce phosphors for warm white light generation. Note that this evaluation does not take into account the non-flat excitation spectrum of GSAG:Ce nor the re-absorption effects. The red component of the GSAG:Ce emission shifts the calculated CIE coordinates towards warmer white light, which corresponds to approximately 3000 K.

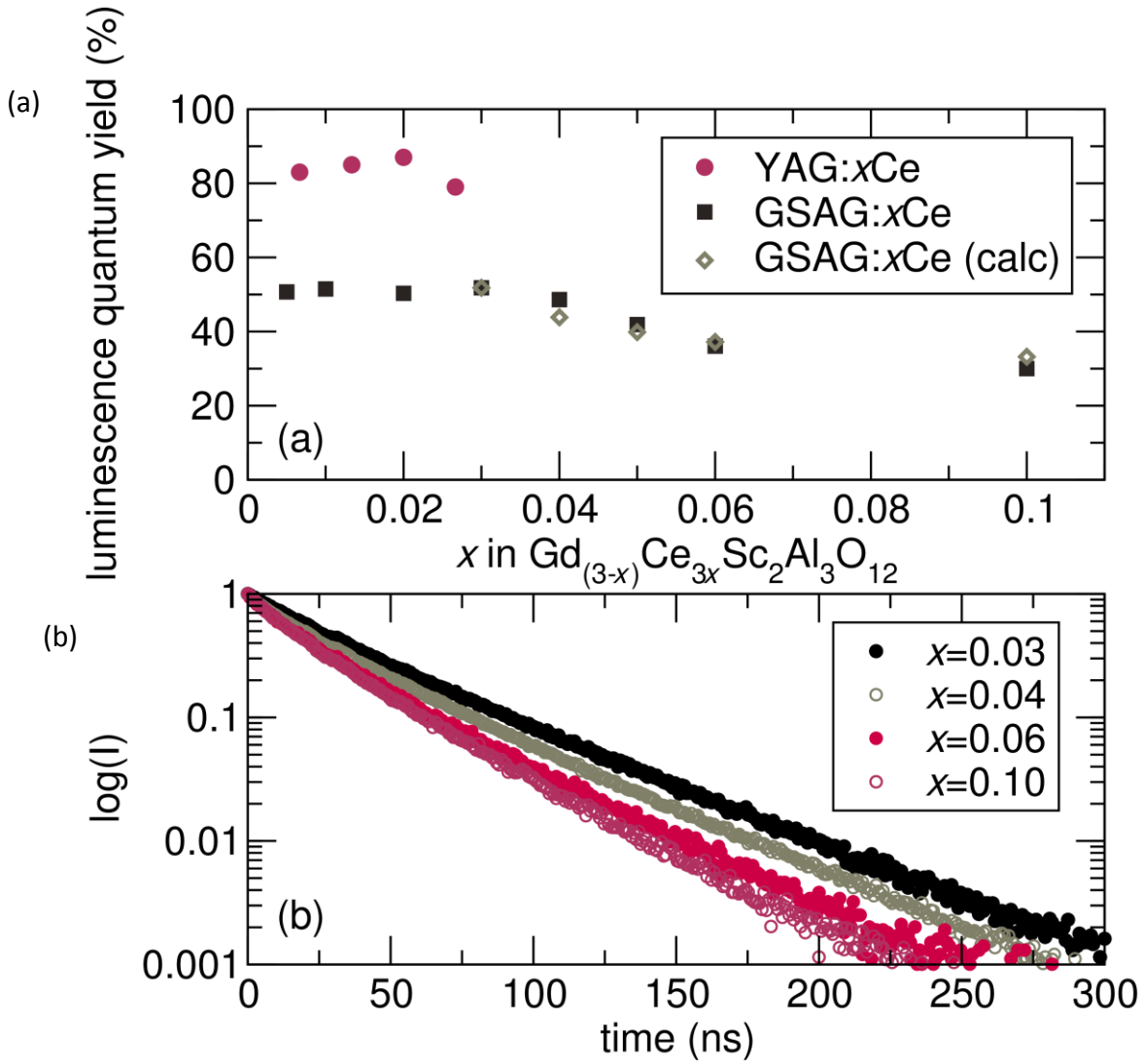

Figure 5. *(a) Evolution of the luminescence quantum yield of YAG:xCe and GSAG:xCe as a function of Ce content x. The quantum yield calculated from the excited state lifetimes [GSAG:xCe (calc)] are shown as empty diamonds. (b)* Ce^{3+} *excited state lifetimes for* $Gd_{3(1-x)}Ce_{3x}Sc_2Al_3O_{12}$ *samples where x= 0.03, 0.04, 0.06 and 0.1.*

The internal luminescence quantum yield (Φ) of GSAG:*x*Ce and YAG:*x*Ce is illustrated in **Figure 5a** as a function of *x*, where Φ is defined as the ratio of the number of the emitted photons over the number of the absorbed photons and is determined using an integrating sphere. For both compounds, the evolution is typical of inorganic powdered phosphors, with a maximum value at the low Ce concentrations, followed by a decrease at higher concentrations due to concentration quenching. This decrease is particularly visible in the case of GSAG:Ce as the Ce doping range is much wider than in the case of YAG:Ce. YAG:Ce is well-known for its high quantum yield, with values above 80 %. Note that commercially available YAG:Ce micron-sized powder can even reach an internal luminescence quantum yield of 95 %. The observed quantum yield of GSAG:Ce is lesser, with a maximum value of 52 % for a doping concentration of x = 0.03.

Lifetime measurements were performed on $Gd_{3(1-x)}Ce_{3x}Sc_2Al_3O_{12}$ as a function of *x* and the decay curves are presented on **Figure 5b**. The decay time values are presented in **Table 1**. At low Ce concentration (*x* = 0.03), the decay curve is single-exponential, evidencing a rather homogeneous distribution of Ce in the GSAG network. As the concentration increases, the decay curves tend to be bi-exponential with a characteristic decay at short times corresponding to Ce-Ce pairs or small clusters.[26] In that case, an average decay time <τ> is evaluated at 25 ns, by taking into account the relative contribution (A_1 and A_2) of the decay constants τ_1 and τ_2 (**Table 1**).

Samples	Decay time (ns)
GSAG:0.03Ce	τ_1 = 39 ns
GSAG:0.04Ce	τ_1 = 33 ns
GSAG:0.05Ce	τ_1 = 30 ns
GSAG:0.06Ce	τ_1 = 28 ns
GSAG:0.10Ce	τ_1 = 10 ns, A_1 = 0.28 and τ_2 = 31 ns A_2 = 0.72

***Table 1**: Lifetimes of the Ce^{3+} excited state in GSAG:xCe. For low concentration samples, a single-exponential fitting ($exp(-t/\tau_1)$) was performed, whereas for the most concentrated sample, a bi-exponential fitting ($A_1 exp(-t/\tau_1) + A_2 exp(-t/\tau_2)$) was necessary.*

The lifetime τ of Ce^{3+} excited state can be correlated to the internal luminescence quantum yield Φ through the following expression: $\Phi = \frac{\tau}{\tau_r}$ (**Eq. 1**) where τ_r corresponds to the radiative lifetime.[27] Considering the GSAG sample doped with 3 mol.% Ce, for which the decay curve is single-exponential, and correlating its values of Φ and τ, one can determine the value of τ_r : τ_r = 84 ns. In YAG, the radiative lifetime of Ce^{3+} is 65 ns.[28] This difference can be explained by the difference of refractive index between the two materials (1.84 for YAG[29] and 1.93 for GSAG[30] at 500 nm) as τ_r can be written as $\frac{1}{\tau_r} = f(ED)\frac{\lambda_0^2}{n(n^2+2)^2}$.

Once τ_r is determined, the theoretical values of Φ for other doping concentrations can be deduced using **Eq. 1**, and are reported in **Figure 5a** (empty diamonds). Good agreement is found between the measured quantum yield Φ and the quantum yield obtained from the lifetime values.

The excited state lifetime τ was measured as a function of temperature for YAG:0.02Ce, GSAG:0.02Ce and GSAG:0.1Ce, as reported in **Figure 6**. This is a well-known method to study the temperature quenching of the emission, as the radiative lifetime of an allowed transition is usually not affected by the temperature change, thus the shortening of the luminescence lifetime indicates the appearance of new non radiative paths.[31,32] In YAG:0.02Ce, τ remains constant on a broad temperature range (100-400 K), in accordance with the study published by V. Bachmann *et al.* who report constant values of τ up to 480 K for YAG:0.01Ce and up to 440 K for YAG:0.033Ce.[33] In GSAG:0.02Ce and GSAG:0.1Ce, the quenching temperature is much lower as τ decreases when the temperature is above 225 K. This behaviour is similar to the one of $Y_3Sc_2AlGa_2O_{12}$ doped with 0.5mol.% Ce.[34]

To explain the evolution of luminescence with increasing temperature, the position of the lowest excited states ($5d^1$ and $5d^2$) of Ce^{3+} with respect to the host conduction band should be considered. J. Ueda *et al.* recently reported the energy level diagrams of YAG:Ce[35] and show the $5d^1$ and $5d^2$ levels of Ce^{3+} are situated inside the energy gap of the YAG matrix, at respectively 0.50 eV and 0.08 eV below the conduction band. The mechanism of thermal ionization from the $5d^1$ level has been determined to occur at temperatures higher than 300°C (573 K). In GSAG:Ce, no data has been presented in the literature to our knowledge. As we observed a red-shift of the emission, attributed to a stronger crystal-field splitting, we expect a $5d^1$ level situated at a lower energy in the band gap of the GSAG matrix. At the same time, the band gap of GSAG is approximately 6.3 eV[13], smaller than that of YAG

(6.5 eV)[35]. To study in more detail the photo-ionization process and the temperature quenching, photoconductivity measurements should be performed; however this is beyond the scope of this paper.

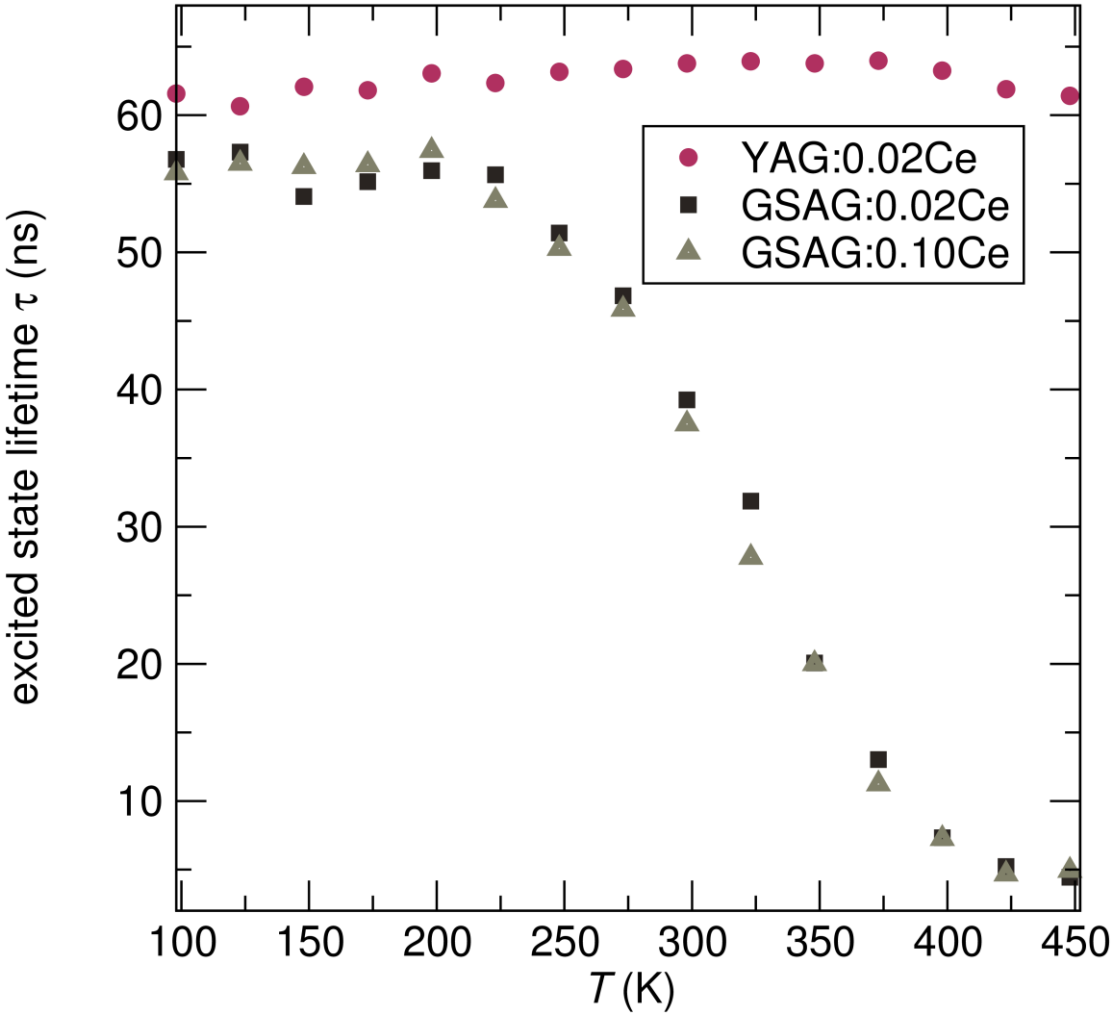

Figure 6. *Evolution of the excited state lifetime of Ce^{3+} in YAG:0.02Ce, GSAG:0.02Ce and GSAG:0.1Ce with temperature.*

4. Discussion

YAG and GSAG compounds crystallize in a cubic structure belonging to the $Ia\bar{3}d$ space group. The structure is composed of AlO_4 tetrahedra, AlO_6 or ScO_6 octahedra, and Y^{3+} or Gd^{3+} in a 8-coordinated site. When doping the YAG matrix with Ce^{3+} ions, the Ce^{3+} occupy the Y^{3+} site.[2] The difference of ionic radius between Y^{3+} (r_{Y3+}=1.019 Å for CN=8) and Ce^{3+} (r_{ce3+}=1.143 Å for CN=8) is of importance, with a difference of about 12%. Consequently, despite having the same charge state, Ce^{3+} ions cannot substitute more than 3 mol. % for the Y^{3+} ions. In GSAG, the size of Gd^{3+} ions (r_{Gd3+}=1.053 Å in CN=8) is slightly bigger than the one of Y^{3+}, which facilitates the insertion of Ce^{3+} ions in the lattice. In addition, in GSAG, Sc^{3+} ions are larger (r_{sc3+}=0.75 Å for CN=6) than Al^{3+} ions (r_{Al3+}=0.54 Å for CN=6), which contributes to an overall larger lattice and as a result the increased solubility of Ce^{3+} in GSAG compared to YAG.

In order to understand more deeply the large incorporation of Ce^{3+} in GSAG, interatomic distances were considered. We specifically focused on the metal (Y or Gd) site, which is the site occupied by the

luminescent doping ion. The Y—O (resp. Gd-O) distances and O···O distances (polyhedron edges) were obtained from literature structures[36,7] using the Gretep software.[19] Those distances were compared to theoretical values obtained by Y-N. Xu *et al.* through local-density calculations.[37] A good agreement is found between the experimental and theoretical reports (**Table 2**).

Interatomic distances and bond number in YAG			**Interatomic distances and bond number in GSAG**		
	Using Gretep	From [37]		Using Gretep	From [37]
Y—O distances	2.303 Å x 4	2.303 Å	Gd—O distances	2.371 Å x 4	2.371 Å
	2.438 Å x 4	2.438 Å		2.478 Å x 4	2.479 Å
O···O distances in the 1st coordination sphere of Y	2.631 Å x 4	2.658 Å	O···O distances in the 1st coordination sphere of Gd	2.704 Å x 2	2.705 Å
	2.717 Å x 2	2.696 Å		2.814 Å x 4	2.815 Å
	2.855 Å x 4	2.837 Å		2.856 Å x 4	2.852 Å
	2.936 Å x 2	-		2.953 Å x 2	-

***Table 2**: Interatomic distances in YAG and GSAG from literature structures,[36,7] calculated using Gretep software[19] and compared with theoretical values from [37]. The O···O distances correspond to the distances between oxygen atoms in the first coordination sphere of Y (resp. Gd) in YAG (resp. GSAG).*

The first coordination sphere around Y (resp. Gd) in YAG (resp. GSAG) is represented in **Figure 7**. In YAG, short oxygen-oxygen distances are found: $d_{O\text{-}O}$ = 2.631 Å, which corresponds to an edge shared with an AlO_6 octahedron, and $d_{O\text{-}O}$ = 2.717 Å, which corresponds to an edge shared with an AlO_4 tetrahedron. Those distances are smaller than the sum of two $r_{O2\text{-}}$ (with $r_{O2\text{-}}$=1.38 Å), indicating that Y is in a compressed site, in accordance with the experimental results obtained in [13]. The average oxygen-oxygen distance for the metal site is 2.77 Å. In GSAG, the shortest oxygen-oxygen distance (2.704 Å) corresponds to an edge shared with an AlO_4 tetrahedron. The edges shared with the ScO_6 octahedra present longer oxygen-oxygen distances (2.814 Å and 2.856 Å), which can be explained by the size of Sc^{3+} (r_{sc3+}=0.75 Å in CN=6), larger than Al^{3+} (r_{Al3+}=0.54 Å in CN=6). The average oxygen-oxygen distance for the metal site is 2.83 Å, i.e. 2.0 % larger than in YAG. Hence, in GSAG, the metal site is less compressed than in YAG, explaining the higher solubility of Ce.

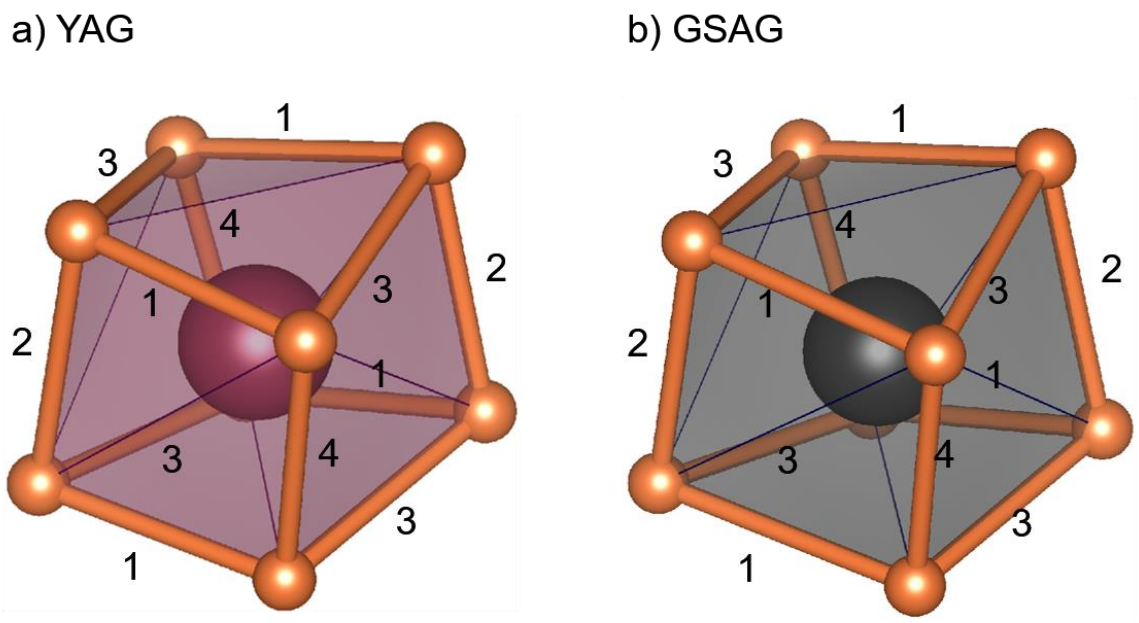

Figure 7. *Representation of (a) the Y site in YAG with bond distances 1 = 2.631 Å, 2 = 2.717 Å, 3 = 2.855 Å, and 4 = 2.936 Å and (b) the Gd sit in GSAG with bond distances 1 = 2.856 Å, 2 = 2.704 Å, 3 = 2.814 Å, and 4 = 2.953 Å.*

The work on GSAG:Ce was initiated in order to investigate the potential of this compound to demonstrate a higher external quantum efficiency (EQE) than YAG:Ce. The direct measurement of the EQE is difficult as it does depend on the phosphor concentration and packaging. A few papers report EQE measurements using a double-integrating sphere, allowing an accurate measurement.[38] The EQE is defined as the ratio of the emitted photons N_{em} over the number of incident photons N_{inc}:

$$EQE = \frac{N_{em}}{N_{inc}} \qquad \text{(Eq. 1)}$$

N_{em} is related to the internal quantum yield Φ by the equation:

$$N_{em} = \Phi\, N_{abs} \quad \text{(Eq. 2)}$$

Where N_{abs} is the number of absorbed photons. We consider the case of a transparent phosphor layer. In that case, N_{abs} can be written as:

$$N_{abs} = N_{incident} - N_{transmitted} - N_{reflected} \quad \text{(Eq. 3)}$$

and is proportional to:

$$N_{abs} \sim I_0\,(1 - \exp\left(\frac{x\,N_A\,d\,t\,\sigma}{M}\right) - R) \qquad \text{(Eq. 4)}$$

I_0 is the incident light intensity, i.e. proportional to N_{inc}, x is the Ce concentration in mol.%, N_A is the Avogadro number, d is the phosphor density in g.cm^{-3}, t its phosphor thickness in cm, M its molar weight in g.mol^{-1}, σ is the absorption cross-section of Ce^{3+} and R is a constant describing the reflection rate. In the approximation of a thin transparent phosphor layer, defined by the product $\left(\frac{x\,N_A\,d\,t\,\sigma}{M}\right) \ll 1$ (i.e. $t < 40$ µm for $x = 0.1$ in GSAG), which is a geometry more and more explored thanks to its limited scattering rate,[39,40] it can be written:

$$EQE \sim \Phi(\frac{x\,N_A\,d\,t\,\sigma}{M} - R) \qquad \text{(Eq. 5)}$$

Taking into account the values of Φ (**Fig. 5a**), the density of YAG and GSAG (4.56 g/cm^3 [41] and 5.72 g/cm^3 [42] resp.), their molar weight (593 g/mol and 834 g/mol resp.) and considering a constant reflection rate *R* for all samples, the theoretical EQE was calculated for $Gd_{3(1-x)}Ce_{3x}Sc_2Al_3O_{12}$ and $Y_{3(1-x)}Ce_{3x}Al_5O_{12}$ and is reported in **Figure 7** as a function of *x*. Note that the value of *x* taken for this calculation is the nominal concentration. According to **Figure 2**, showing that the unit cell parameter of GSAG:*x*Ce perfectly follows the Vegard's law for *x* varying between 0 and 0.1, this seems to be appropriate.

The expected EQE with YAG:Ce is higher than that of GSAG:Ce at the same Ce concentration. However, a maximum EQE is obtained for GSAG:0.1Ce, a doping level which cannot be achieved in YAG due to the solubility limit of Ce^{3+} in YAG. At this level of Ce-doping, the generation of photons is approximately 30% more than YAG:0.02Ce, assuming the same amount of phosphor is used. The evolution of the calculated EQE curve of GSAG:*x*Ce is not linear. In particular, one can notice a slow down for $x = 0.06$ and a high EQE value for $x = 0.1$. This behaviour results from the fact that GSAG:0.06Ce and GSAG:0.1Ce exhibit similar intrinsic quantum yield (**Figure 5**) but the doping concentration is 40% higher in GSAG:0.1Ce. Note that all these calculations are valid under the approximation of thin transparent phosphor layers. For an experimental proof, it would be necessary to work with a non-conventional geometry, where GSAG:Ce or YAG:Ce phosphors would not be encapsulated inside an epoxy dome but would form a transparent thin layer (thickness < 40 µm for GSAG:0.1Ce according to the calculations explained above).

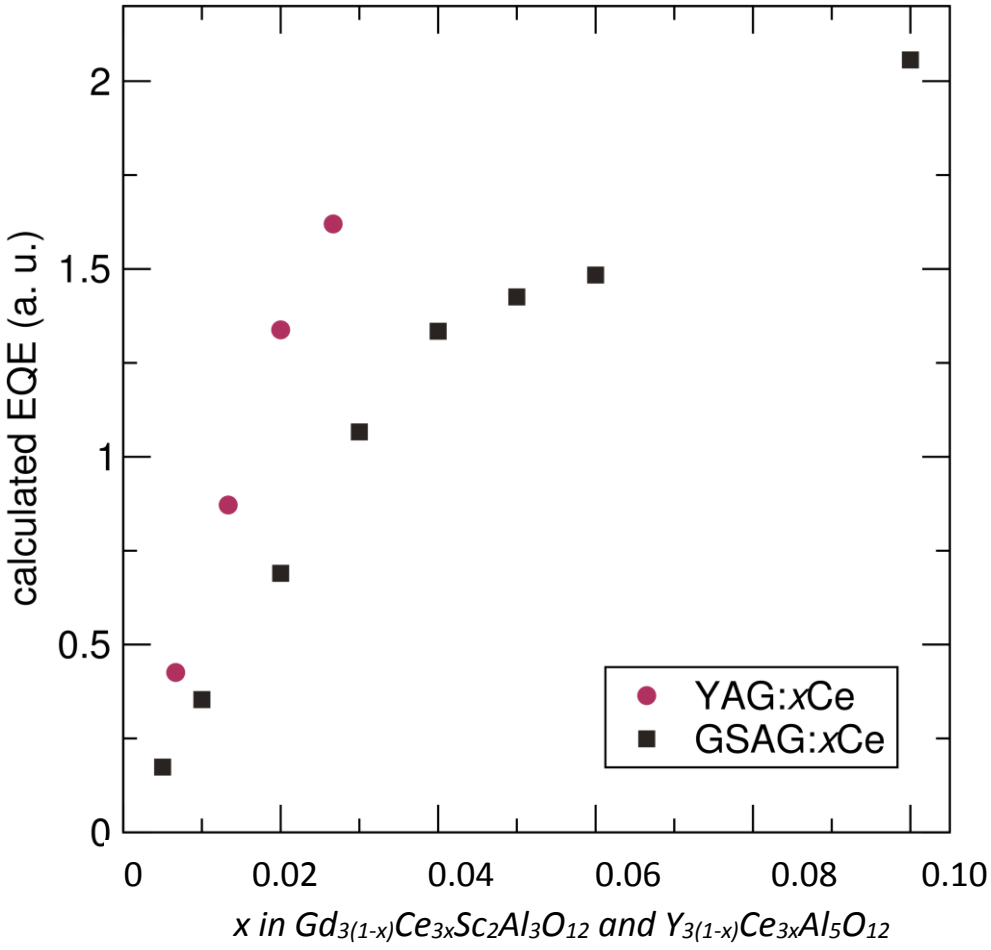

Figure 8. *Evolution of the calculated EQE corresponding to the product of Φ and the Ce concentration x in $Gd_{3(1-x)}Ce_{3x}Sc_2Al_3O_{12}$ and $Y_{3(1-x)}Ce_{3x}Al_5O_{12}$ as a function of x. While YAG possesses a higher EQE than GSAG at the same doping level, the highest EQE is achieved for GSAG:0.10Ce, a doping level which cannot be realized in YAG.*

5. Conclusion

Thanks to its intrinsic crystal structure and more specifically a large metal site (GdO_8 polyhedron), $Gd_3Sc_2Al_3O_{12}$ can incorporate up to 18 mol.% Ce^{3+}, i.e. up to six times more than YAG where the metal site is more compressed. With doping concentration of 10 mol.% Ce^{3+}, a thin transparent layer of GSAG:Ce phosphors should exhibit an external quantum yield 30% higher than the corresponding layer of YAG:Ce. Such layers, with a typical thickness of 40 µm, could be prepared using GSAG:Ce nanoparticles, which will be considered in future work.

This study, presented in the case of phosphors for white LED-based lighting, highlights the fact that the figure of merit is not always the material internal quantum yield. If a limited quantity of matter is to be used, the key factor is the material brightness, i.e. the EQE. So, going beyond the case of GSAG, whose applicability is limited by a lower temperature quenching than YAG, this study evidences that research for improved phosphor performance can be driven by the compromise between a high internal quantum yield and a high activator concentration leading to the optimal EQE efficiency. An interesting question that remains open is to determine whether a crystal structure could reconcile a high doping concentration with a high internal quantum yield.

Acknowledgments

The authors would like to thank Prof. A. Petrosyan for fruitful discussions on garnet structure. This research is partly conducted in the scope of the International Associated Laboratory (CNRS–France & SCS–Armenia) IRMAS

[1] S. Nishiura, S. Tanabe, K. Fujioka, Y. Fujimoto, Properties of transparent Ce:YAG ceramic phosphors for white LED, *Opt. Mater*. **33**, 2011, 688-691

[2] N.C. George, A.J. Pell, G. Dantelle, K. Page, A. Llobet, M. Balasubramanian, G. Pintacuda, B.F. Chmelka, R. Seshadri, Local Environments of Dilute Activator Ions in the Solid-State Lighting Phosphor $Y_{3-x}Ce_xAl_5O_{12}$, *Chem. Mater*. **25***,* 2013**,** 3979-3995

[3] T. Hussain, L. Zhong, M. Danesh, H. Ye, Z. Liang, D. Xiao, C-W. Qiu, C. Lou, L. Chi, L. Jing, Enabling low amounts of YAG:Ce(3+) to convert blue into white light with plasmonic Au nanoparticles *Nanoscale* **7**, 2015**,** 10350-10356

[4] N. Pannier, M. Filoche, M. Plapp, V. Buissette, T. Le Mercier, Modeling the role of phosphor grain packing in compact fluorescent lamps, *Proceedings of SPIE* , **8129**, 2011, 81290D

[5] A. Revaux, G. Dantelle, N. George, R. Seshadri, T. Gacoin, J.P. Boilot, A protected annealing strategy to enhanced light emission and photostability of YAG:Ce nanoparticle-based films, *Nanoscale* **3**, 2011, 2015-2022

[6] A. Revaux, G. Dantelle, D. Decanini, A.M. Haghiri-Gosnet, T. Gacoin, J.P. Boilot, Synthesis of YAG:Ce/TiO_2 nanocomposite films, *Opt. Mater.* **33**, 2011, 1124-1127

[7] S. Yamazaki, F. Marumo, K. Tanaka, H. Morikawa, N. Kodama, K. Kitamura, Y. Miyazawa, A structural study of facet and off-facet parts of rare-earth garnets, $Gd_3Sc_2Al_3O_{12}$, $Gd_3Sc_2Ga_3O_{12}$, *J. Solid. State Chem.* **108**, 1994, 94-98

[8] B. Struve, P. Fuhrberg, W. Luhs, G. Liftin, Thermal lensing and laser opteration of flashlamp-pumped Cr:GSAG, *Opt. Comm.* **65**, 1988, 291-296

[9] A.N. Alpat'ev, E.V. Zharikov, A.I. Zagumennyĭ, D.A. Zubenko, S.P. Kalitin, G.B. Lutts, M.A. Noginov, V.A. Smirnov, A.F. Umyskov, I.A. Shcherbakov, Holmium GSAG:Cr^{3+}:Tm^{3+}:Ho^{3+} crystal laser (λ = 2.09 µm) operating at room temperature, *Sov. J. Quantum Electron.* **19**, 1989, 1400-1402

[10] S.G.P. Strohmaier, H.J. Eichler, C. Czeranowsky, B. Ileri, K. Pertmann, G. Huber, Diode pumped Nd:GSAG and Nd:YGG laser at 942 and 935 nm, *Opt. Comm.* **275**, 2007, 170-172
[11] A. Kling, D. Kollewe, D. Mateika, Scintillation properties of cerium-doped gadolinium-scandium-aluminum garnets, *Nuclear Instr. Meth. In Phys. Research A* **346**, 1994, 205-212
[12] N.J. Cherepy, S.A. Payne, S.J. Asztalos, G. Hull, J.D. Kuntz, T. Niedermayr, S. Pimputkar, J.J. Roberts, R.D. Sanner, T.M. Tillotson, E. van Loef, C.M. Wilson, K.S. Shah, U.N. Roy, R. Hawrami, A. Burger, L.A. Boatner, W.S. Choong, W.W. Moses, Scintillators with Potential to Supersede Lanthanum Bromide, *IEEE Transactions on Nuclear Science* **56**, 2009*,* 873
[13] U. Happek, J. Choi, A.M. Srivastava, Observation of cross-ionization in $Gd_3Sc_2Al_3O_{12}:Ce^{3+}$ *J. Lumin.* **94-95,** 2001*,* 7-9
[14] A. Birkel, K.A. Denault, N.C. George, C.E. Doll, B. Hery, A.A. Mikhailovsky, B.C.S. Birkel, B.C. Hong, R. Sechadri, Rapid Microwave Preparation of Highly Efficient Ce^{3+}-Substituted Garnet Phosphors for Solid State White Lighting, *Chem. Mater.* **24(6),** 2012, 1198-1204
[15] A. Le Bail, Whole pattern decomposition methods and applications: a retrospection, *Powder Diffr.* **20**, 2012, 316–326
[16] A.C. Larson, R.B. Von Dreele, General Structure Analysis System (GSAS), *Los Alamos Nat. Lab. Rep.* 1994, *LAUR*, 89–748.
[17] B.H. Toby, EXPGUI, a graphical user interfacefor GSAS ,*J. Appl. Crystallogr.* **34**, 2001, 210–213
[18] K. Momma, F. Izumi, VESTA 3 for three-dimensional visualization of crystal, volumetric and morphology data, *J. Appl. Crystallogr*. **44**, 2001, 1272-1276
[19] http://www.ccp14.ac.uk/tutorial/lmgp/gretep.html
[20] E. Homeyer, S. Pailhès, R. Debord, V. Jary, C. Dujardin, G. Ledoux, Diamond contact-less micrometric temperature sensors, *Appl. Phys. Lett.* **106,** 2015, 243502
[21] J.M. Robertson, M.W. van Tol, H.M. Smits, J.P.H. Heynen, Colourshift of the Ce3+ emission in monocrystalline epitaxially grown garnet layers, *Philips J. Res.* **36**, 1981, 15-30
[22] J.L. Wu, G. Gundiah, A.K. Cheetham, Structure–property correlations in Ce-doped garnet phosphors for use in solid state lighting, *Chem. Phys. Lett.* **441**, 2007, 250-254
[23] G. Gaudiah, Y. Shimomura, N. Kijima, A.K. Cheetham, Novel red phosphors based on vanadate garnets for solid state lighting applications, *Chem. Phys. Lett.* **455**, 2008, 279-283
[24] A.A. Setlur, W.J. Heward, Y. Gao, A.M. Srivastava, R.G. Chandran, M.V. Shankar, Crystal Chemistry and Luminescence of Ce^{3+}-Doped $Lu_2CaMg_2(Si,Ge)_3O_{12}$ and Its Use in LED Based Lighting, *Chem. Mater.* **18**, 2006, 3314-3320
[25] R. Le Toquin, A.K. Cheetham, Red-emitting cerium-based phosphor materials for solid-state lighting applications, *Chem. Phys. Lett.* **423**, 2006, 352-356
[26] E. Maurice, G. Monnom, B. Dussardier, D.B. Ostrowsky, . Clustering effects on double energy transfer in heavily ytterbium–erbium-codoped silica fibers, *J. Opt. Soc. Am. B* **13(4)***,* 1996, 693-701
[27] K. Binnemans, Lanthanide-based luminescent hybrid Materials. *Chem. Rev.* **109,** 2009, 4283-4374
[28] K.V. Ivanovskikh, J.M. Ogiegło, A. Zych, C.R. Ronda, A. Meijerink, A. Luminescence Temperature Quenching for Ce^{3+} and Pr^{3+} d-f Emission in YAG and LuAG, *ECS J. Solid State Science and Technology*, **2(2),** 2013, R3148-R3152
[29] D.E. Zelmon, D.L. Small, R. Page, Refractive-index measurements of undoped yttrium aluminum garnet from 0.4 to 5.0 mm, *Applied Optics* **37(21),** 1998, 4933-4935
[30] J. Su, B. Liu, L.H. Xu, Q.L. Zhang, S.T. Yin, Effective segregation during Czochralski growth and spectral properties of Nd^{3+} in GSAG crystal, *J. Alloys Comp.* **512,** 2012, , 230-234
[31] G. Blasse, B.C. Grabmaier, B.C. « Luminescent Materials » Springer-Verlag, Berlin, **1994**
[32] P. Dorenbos, The $4f^n \leftrightarrow 4f^{n-1}5d$ transitions of the trivalent lanthanides in halogenides and chalcogenides, *J. Lumin.* **91,** 2000, 91
[33] V. Bachmann, C. Ronda, A. Meijerink, Temperature Quenching of Yellow Ce^{3+} Luminescence in YAG:Ce, *Chem. Mater.* , **21**, 2009, 2077-2084

[34] J. Ueda, K. Aishima, S. Tanabe, Temperature and compositional dependence of optical and optoelectronic properties in Ce^{3+}-doped $Y_3Sc_2Al_{3-x}Ga_xO_{12}$ (x = 0, 1, 2, 3), *Opt. Mater.* **35,** 2013, 1952-1957

[35] J. Ueda, S. Tanabe, T. Nakanishi, Analysis of Ce^{3+} luminescence quenching in solid solutions between, $Y_3Al_5O_{12}$ and $Y_3Ga_5O_{12}$ by temperature dependence of photoconductivity measurement, *J. Appl. Phys.* **110,** 2011, 053102

[36] A. Emiraliev, A.G. Kocharov, R.V. Bakradze, U. Karimov, Z.I. Ahmetzhanov, The neutron diffraction redefinition of the coordinates of the atoms of oxygen in yttrio-aluminium garnet, *Soviet Physics Crystallography* **21**, 1976, 112-113

[37] Y.N. Xu, W.Y. Ching, B.K. Brickeen, Electronic structure and bonding in garnet crystals $Gd_3Sc_2Ga_3O_{12}$, $Gd_3Sc_2Al_3O_{12}$, and $Gd_3Ga_3O_{12}$ compared to $Y_3Al_3O_{12}$, *Phys. Rev. B* **61(3),** 2000, 1817-1824

[38] Z. Liu, S. Liu, K. Wang, X. Luo, Measurement and numerical studies of optical properties of YAG:Ce phosphor for white light-emitting diode packaging *Appl. Optics* **49(2),** 2010, 247-257

[39] H. Menkara, R.A. Gilstrap, T. Morris, M. Minkara, B.K. Wagner, C.J. Summers, Development of nanophosphors for light emitting diodes, *Opt. Expr.* **19**, 2011, A972

[40] C. Hu, Y. Shi, X. Feng, Y. Pan, YAG:Ce/(Gd,Y)AG:Ce dual-layered composite structure ceramic phosphors designed for bright white light-emitting diodes with various CCT, *Opt. Express* **23(14)**, 2015, 18243

[41] M. Nikl, Scintillation detectors for x-rays, *Meas. Sci. Technol.* **17**, 2006, R37–R54

[42] G.B. Lutts, A.L. Denisov, E.V. Zharikov, A.I. Zagumennyi, S.N. Kozlikin, S.V. Lavrishchev, S.A. Samoylova, GSAG and YSAG: a study on isomorphism and crystal growth, *Opt. Quant. Electronics* **22,** 1990, S269-S281

Graphical abstract